(Received 4 July 2024, Accepted 20 August 2024, Scheduled 2 September 2024)

3D-Printing of Slanted Corrugated Horn Antennas for the E-Band

Markus Tafertshofer[1, *], Maximilian Binder[2], and Erwin Biebl[1]

[1] TUM School of Computation, Information and Technology, Germany
[2] Heidenhain GmbH, Germany

ABSTRACT: In this paper, the feasibility of using additive manufacturing (AM) technologies for the fabrication of corrugated horn antennas for the E-band (60 to 90 GHz) is investigated. Stereolithography apparatus (SLA) and selective laser melting (SLM) are identified as the most suitable technologies for manufacturing horn antennas in this frequency range. To ensure good manufacturing, slanted corrugations are utilized. The antennas have a gain of 13 dBi at 72 GHz and are designed in CST Microwave Studio. For the fabrication of the plastic parts, SLA and the finer-scaled projection micro stereolithography (PμSL) technology are applied. The metal antennas are printed with direct metal laser sintering (DMLS) from the aluminum alloy $AlSi_{10}Mg$ and the finer scaled micro metal laser sintering (μMLS) from 316L stainless steel. Overall, four antennas are fabricated. The plastic antennas are plated with copper. Dimensional tolerances and surface roughness of the antennas are evaluated. The antennas are investigated considering H- and E-plane beam shapes, input reflection, and realized gain. The measurement is conducted in an anechoic chamber using the Single-Antenna method. The μMLS antenna supplies the best results.

1. INTRODUCTION

Additive manufacturing (AM) technologies, also referred to as 3D printing, gradually receive more attention as possible alternative manufacturing technologies for millimeter-wave (mmW) devices (30–300 GHz). The fabrication of mmW waveguide components requires sophisticated manufacturing processes, e.g., milling, micromachining, or injection molding. Many of these conventional processes build parts in a subtracting manner. Contrary to those, in AM, parts are fabricated in an additive manner, layer by layer. Compared to conventional manufacturing techniques, less waste is generated; most of the unused material can be recycled; and less power is consumed. Additionally, no mask, tooling, or molding-related cost emerges, which results in a reduced overall cost and shorter turn-around time. Both metallic and plastic AM technologies are worth considering for manufacturing waveguide components. Plastic components are advantageous in lightweight applications but cause more process complexity since metal plating is required. Metal AM parts profit from physical rigidness and reduced process complexity compared to their plastic counterparts. However, the surface quality of metal AM parts is generally worse than that of plastic parts. There are many researches in waveguide antennas currently, for example, in the field of ultra-wideband antennas, as reported in [1] and [2]. More complex antenna shapes for coaxial connection [3] or integrated substrate waveguide antennas [4] are also of interest. Various AM fabricated standard horn antennas have been reported in [5–11], for example. Most of the reported antennas for frequencies above 60 GHz are printed from a polymer or rely on mechanical post-processing. However, emerging technologies allow designs to the sub-terahertz domain [12].

The focus of this paper lies in the evaluation of corrugated horn antennas in the E-band (60–90 GHz) printed in different technologies. The antennas will be used in radar target generators to test automotive radars. This work shows that slanted corrugations are suitable for the manufacturing of horn antennas in a practical approach. Furthermore, two major challenges in the procurement of horn antennas should be addressed in this work. They have long delivery periods and high costs. To the authors' knowledge, there is no work evaluating and comparing polymer and metal 3D-printed slanted corrugated horn antennas in this frequency range.

The paper is organized as follows. In Section 2, fundamental AM technologies are introduced, and the most suitable technologies are identified. In Section 3, the design process of the antennas is presented. This is followed by a visual inspection of the manufactured antennas in Section 4, together with an analysis of surface roughness and dimensional tolerance. In Section 5, the Single-Antenna method for gain measurement is introduced; the measurement setup is described; and the results are presented and discussed. Section 6 provides a conclusion and summarizes the work.

2. ADDITIVE MANUFACTURING TECHNOLOGIES

With AM, it is possible to create complicated products with features that cannot be manufactured by common techniques [13]. The geometry of a part is generated in a layer-by-layer manner by subsequently adding voxels [13]. The American Society for Testing and Material (ASTM), together with the In-

* Corresponding author: Markus Tafertshofer (markus.tafertshofer@tum.de).

ternational Organization for Standardization (ISO), classifies seven categories of AM [14]. Nowadays, a wide range of technologies exist which are based on these fundamental technologies. For this work, *vat photopolymerization* and *powder bed fusion* (PBF) are considered. This section provides some factors which are essential for the printing quality. Furthermore, the utilized printing processes and their corresponding process parameters are introduced.

2.1. AM Technologies for mmW Design

General remarks on 3D printing technologies for millimeter-wave design are discussed in [15]. In the following, a short summary of the most important points of [15] is given. The most dominant factors in terms of fabrication accuracy in 3D printing technology are dimensional tolerance and surface roughness. Dimensional tolerance is determined by the powder particle size or the viscosity of the polymer resin, thermal structure changes, laser or electron beam size, and movement control of the printing head. Surface roughness is determined by the same parameters and the melting temperature of the powder. A higher melting point leads to less attachment of surrounding particles, which leads to better surface quality. Post-processing, such as mechanical and chemical polishing, micromachining, or electroplating, can improve the quality but is especially not possible for complex structures. For plastic printing technologies, stereolithography apparatus (SLA), a subcategory of vat photopolymerization, has low tolerance and high surface quality and is, therefore, a good choice for mmW design. For metal AM, selective laser melting (SLM), a subcategory of PBF, outperforms the remaining manufacturing technologies in terms of surface roughness and accuracy. An antenna is printed in a normal SLA process in micro resolution, and a second one is printed in an SLA process called *Projection Micro Stereolithography* (PμSL). The utilized metal AM processes are *Direct Metal Laser Sintering* (DMLS) and a finer version called *Micro Metal Laser Sintering* (μMLS). The process parameters according to the manufacturers are summarized in Table 1. The μMLS process shows the tightest tolerances, followed by the PμSL process. Both of them provide very high resolution. The SLA and DMLS antenna provide higher tolerances and coarser resolution. Further decisions have to be made according to building volume. The two finer processes provide much smaller building volumes than the coarser ones. Another important point that must be considered is the geometry of the print. Due to the layer-by-layer printing method, horizontal overhangs are hard to print in high quality because those structures tend to bend downwards. A solution to this problem can be provided by removable stabilizing structures, but with small structures, it becomes hard to remove them after printing. This brings in slanted corrugations, which will be further discussed in Section 3.2.

TABLE 1. Parameters of the utilized printing techniques.

Process	Dim. tol./μm	Res. z-dir./μm	Res. xy/μm
SLA [16]	100	203	63.5
PμSL [17]	25	5	10
DMLS [18]	200	20	381
μMLS [19, 20]	20	5	30

3. ANTENNA DESIGN PROCESS

The design process of corrugated horn antennas is presented in detail in [21, 22]. Therefore, only the most important parameters of the antennas are given. The antennas are designed using Computer Simulation Technology (CST) Microwave Studio in combination with MATLAB.

3.1. Design Parameters

Every antenna is designed with a nominal gain of $G = 13\,\text{dBi}$ at $f = 72\,\text{GHz}$. The resulting design parameters for the 13 dBi antennas are depicted in Table 2. For better assignment of the values, the schematic of a conical horn is provided in Fig. 1, and the schematic of the corrugations is depicted in Fig. 2. A rectangular WR12 waveguide is used as a feeding structure. The parameter a_i describes the circular waveguide radius and a_o the aperture radius. A mode converter between the WR12 waveguide and circular waveguide is added to transform the TE10 mode to the TE11 mode.

For the corrugations, p_c denotes the pitch width, and w_c describes the groove width. The teeth thickness t_c is chosen to be $0.208\,\text{mm}$, as this is the smallest feature size the utilized PBF machines can resolve. To the authors' knowledge, no mono-

TABLE 2. Design parameters for proposed horn antennas.

Parameter	Corr. Horn
G	13 dBi
a_i	1.988 mm
a_o	3.422 mm
p_c	0.694 mm
t_c	0.208 mm
w_c	0.486 mm
d_c	1 mm
Number of Slots	20
Mode Converter Slots	5

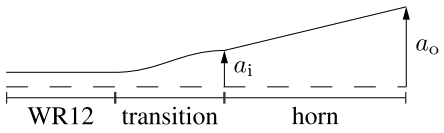

FIGURE 1. Schematic of the antenna without corrugations.

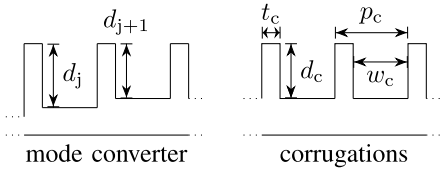

FIGURE 2. Schematic of the variable-depth-slot mode converter and the corrugations [23].

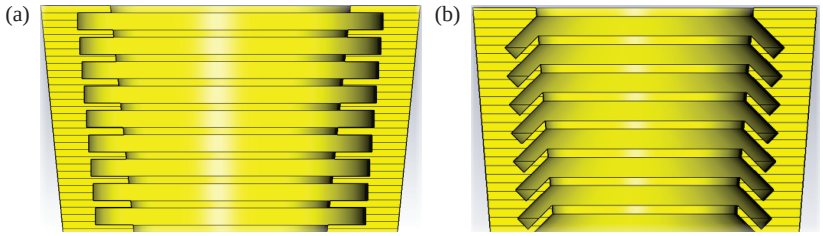

FIGURE 3. Corrugations in antenna design with (a) showing conventional corrugations and (b) showing the adapted slanted corrugation design [23].

lithic corrugated horn antennas for the E-band with such a small pitch width have been reported yet. The groove depth d_c equals $\lambda/4$. The number of corrugations is equal to $N = 20$. Another mode converter is added to convert the field distribution from the TE11 mode of a conical horn to the hybrid HE11 mode of a corrugated horn. In this work, a variable-depth-slot mode converter [22] with a number of slots $N_{MC} = 5$ is implemented. A schematic of this converter is provided in Fig. 2, where d_j denotes the slot depth computed with the formulas of [22]. This converter is added between the rectangular to the conical converter and the beginning of the corrugated horn antenna. The slot depth decreases with every added slot. Further considerations to the design of these corrugated horn antennas can be found in [23].

3.2. Slanted Corrugations

In consultation with the 3D printing service providers, it turns out that conventional corrugated horn antennas with 90° corrugations, as depicted in Fig. 3(a), are not feasible to be manufactured with guaranteed quality, because they tend to bend downwards as already mentioned in Section 3.1. Support structures for stabilization, which can be removed afterward, are not possible with a monolithic design for such delicate structures. Therefore, the design is adapted as depicted in Fig. 3(b). The corrugations are slanted by 45° to the vertical printing direction. Thereby, 90° overhanging printing is avoided, and the structure will stabilize itself [23]. Even if the slanted corrugations start to sag a little, the influence on the results will be very low.

3.3. Simulation

All antennas are simulated using respective surface materials, copper, aluminum, and 316L stainless steel, and the expected surface quality of the corresponding printing process. A yield analysis is conducted to include dimensional tolerances. The results show that the material has little effect on reflection coefficient and antenna patterns, whereas the antenna efficiency will degrade from copper to aluminum to stainless steel, as expected. Due to the corrugation, the field disconnects from the antenna walls, as can be seen in Fig. 4, which shows that the corrugations work as intended. The mode conversion with progressive wave propagation is also observable. Fig. 5 depicts the maximum cross-polarization level. It can be seen that the level increases from 82 GHz to 90 GHz, because the corrugations are optimized for the lower frequencies of the E-band, which is a

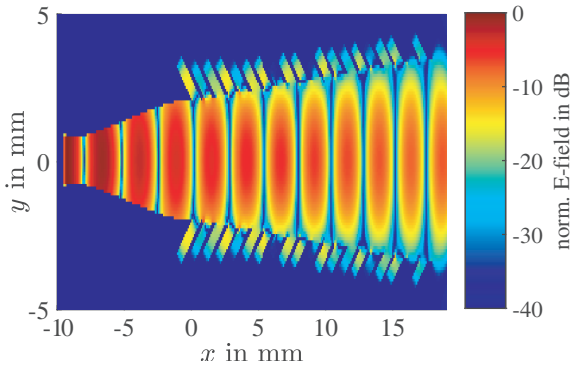

FIGURE 4. E-field inside the antenna side cut.

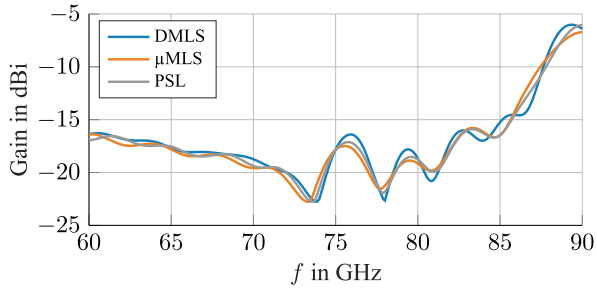

FIGURE 5. Simulation results of maximum cross-polarization gain over frequency.

constraint coming from the manufacturing parameters. This is not a problem for the intended application, as the frequency range used is between 76 GHz and 82 GHz. The highest cross-polarization distance can be found at 78 GHz with about 35 dB difference from the co-polarization gain curve. The E- and H-plane patterns, as well as the cross-polarization patterns, are depicted in Fig. 6. As expected, the gain increases, and the beam width decreases with increasing frequency. Analyzing the patterns at 80 and 90 GHz, it can be seen that sidelobes occur. In comparison to the horn antenna without corrugations, where these sidelobes already occur at 60 GHz and have a maximum distance to the main lobe of 18.8 dB for the E- and 38.7 dB for the H-plane at 60 GHz, a high reduction of the sidelobes can be seen.

4. INSPECTION OF MANUFACTURED ANTENNAS

The antennas are manufactured in SLA and the more accurate processes PµSL from polymer and in DMLS from $AlSi_{10}Mg$

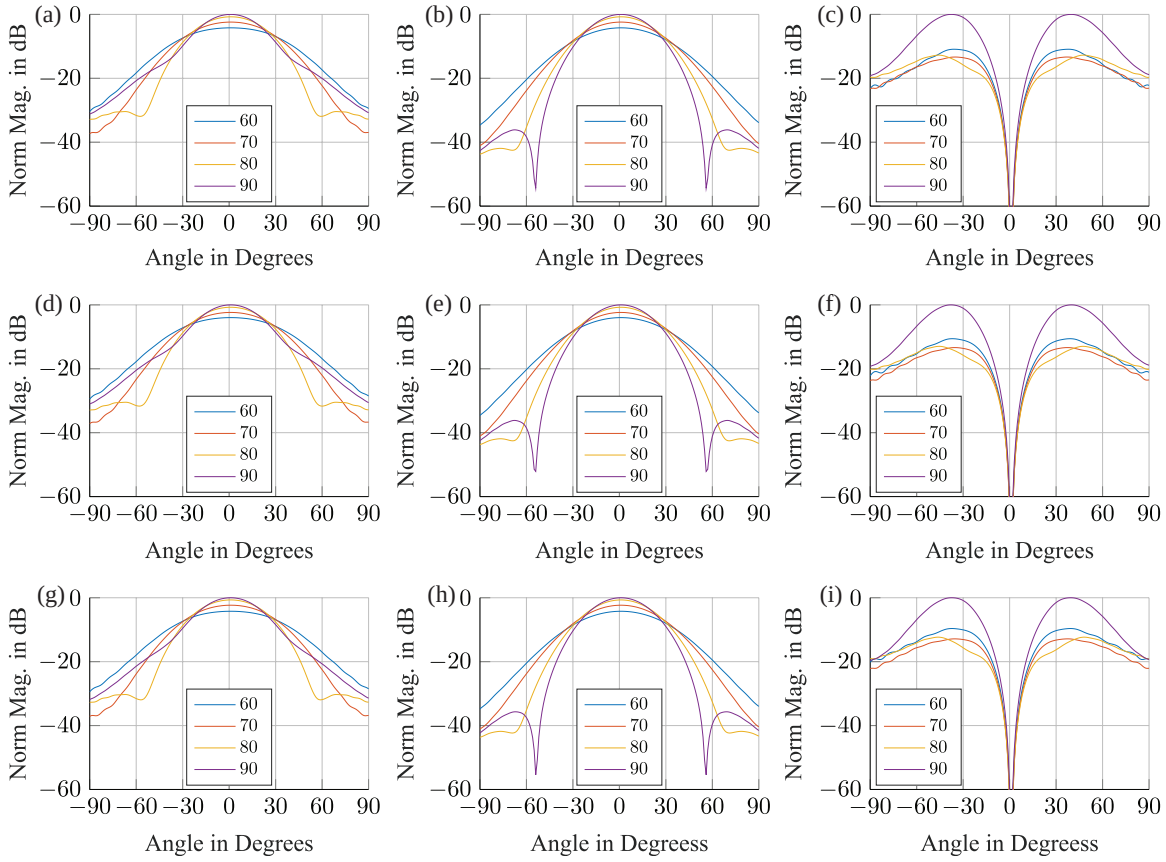

FIGURE 6. Normalized (to max) gain patterns of (a) E-plane, (b) H-plane, (c) 45°-cross-pol. DMLS, (c) E-plane, (d) H-plane, (e) 45°-cross-pol. PµSL, and (d) E-plane, (e) H-plane, (f) 45°-cross-pol. µMLS corrugated horn antennas from 60–90 GHz.

TABLE 3. Overview of the manufactured antennas.

Technology	Material	Cost/€
hline SLA	Microfine Green	561
PµSL	BMF HEK	759
DMLS	$AlSi_{10}Mg$	70
µMLS	316L	2500

TABLE 4. Measured dimensional tolerances (in µm) of antennas.

	waveguide short	waveguide long	$a_{o,corr}$
PµSL	+4	−37	+392
µMLS	−12	−4	+32
DMLS	+56	+148	+191
SLA	−1	−28	+143

and the finer µMLS process from 316L. Overall, four antennas are fabricated. An overview of the antennas and the cost, including the galvanization process, is given in Table 3.

4.1. Measured Dimensional Tolerance

For the measurement of dimensional tolerances, the waveguide input dimensions a and b and the aperture diameters of the corrugated horn antennas and $a_{o,corr}$ are considered. The measurement is conducted using a microscope with corresponding measurement software, as shown in Figs. 7(a)–(d) for the waveguide port of the antennas. The specified dimensions of the WR12 waveguide port are 3.0988 mm width and 1.5494 mm height. The dimensional tolerances are provided in Table 4. The PµSL antenna shows higher dimensional tolerance at the waveguide than specified by the manufacturer. For the aperture diameter of the PµSL antenna, the tolerances are orders of magnitude higher than expected. This may be a result of the plating process, where chemicals might have reacted with the polymer, resulting in a larger diameter. The µMLS antenna has the tightest dimensional tolerances overall, with the waveguide being in tolerance and the aperture diameter being slightly over the specified maximum deviation. The aluminum DMLS horn shows overall the largest dimensional deviations. As expected, the normal SLA part shows small deviations, but the manufacturer's specifications are also partially exceeded.

4.2. Surface and Quality

For surface and quality examination, a visual inspection is provided. Afterwards, the surface roughness is measured using a white-light interferometer. Comparing the resolution of the corrugations in Fig. 8, it can be seen that the PµSL antenna in Fig. 8(b) provides the most accurate results followed by the

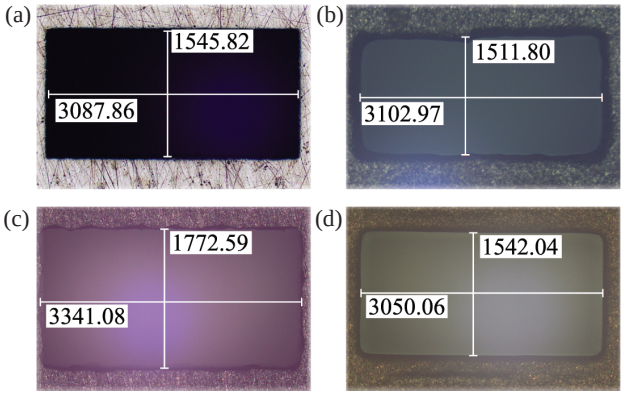

FIGURE 7. Measurement of the waveguide dimensions in µm of (a) µMLS, (b) PµSL, (c) aluminum DMLS and (d) SLA antenna. The WR12 waveguide flange is specified with 3.0988 mm × 1.5494 mm. Additionally, the surface roughness in the waveguide port can be estimated.

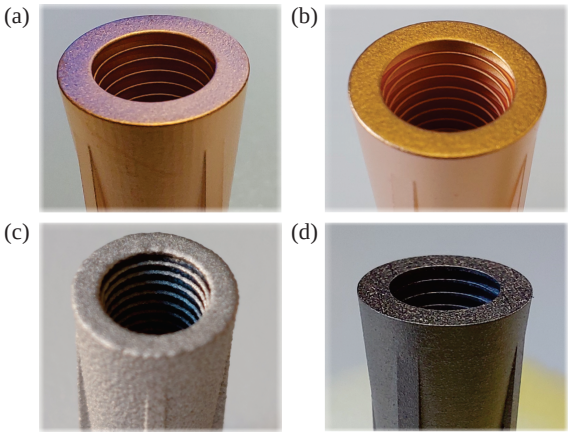

FIGURE 8. Resolution of slanted corrugations for (a) SLA, (b) PµSL, (c) DMLS and (d) µMLS printed antennas.

SLA and µMLS antennas depicted in Fig. 8(a) and 8(d), respectively. As the DMLS antenna, provided in Fig. 8(c), is course-grained, the corrugation accuracy is also very low compared to the other printing technologies. Furthermore, the waveguide flange has to be sanded down, to ensure a good connection to the measurement setup. The material of the SLA-printed corrugated horn antenna called "microfine green" is not successfully plated with copper, as can be seen in Fig. 9. For this reason, the antenna is not considered in the further course.

Measuring the surface of the different antennas with a white-light interferometer provides the results presented in Fig. 10. The measurement is conducted on the top front of the respective antenna. For the µMLS antenna, the traverse paths of the manufacturing laser are recognizable, as can be seen in Fig. 10(a). The light color in the image of the PµSL antenna depicted in Fig. 10(c) shows that the surface is comparatively smooth. The intention maps in the right column show the corresponding height values of the measured section.

Once more, it is recognizable that the PµSL antenna provides the best result in terms of surface roughness, followed by the

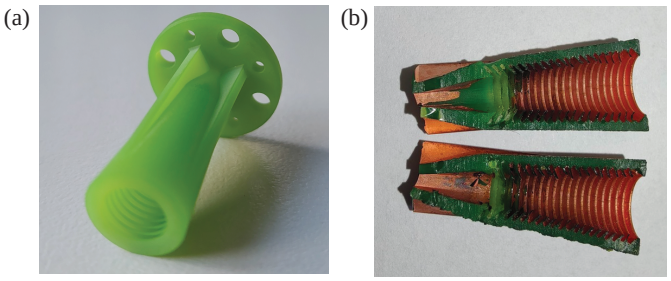

FIGURE 9. SLA printed antenna (a) before copper plating and (b) failed galvanization inside the antenna.

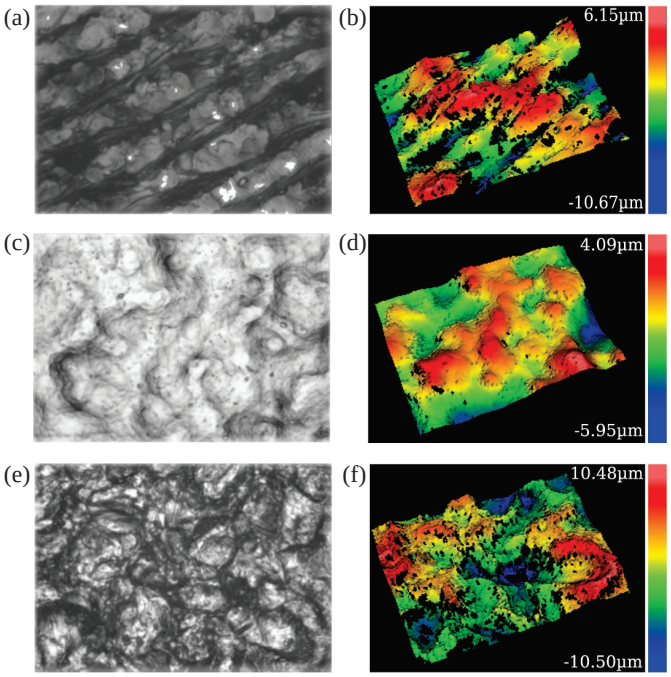

FIGURE 10. Intensity map and corresponding height profile of (a), (b) µMLS [23], (c), (d) PµSL and (e), (f) DMLS antennas..

µMLS antenna. The values of the average surface roughness R_a and RMS surface roughness R_q are provided in Table 5. The values confirm the earlier visual observations for the SLA and PµSL antennas. The values for the DMLS antenna are not representative of the surface quality inside the antenna, where the manufacturer provides values of $R_a = 6.6 - 9.9\,\mu m$ for slanted walls [18].

TABLE 5. Surface roughness measurement.

	µMLS	PµSL + Cu	DMLS	SLA + Cu
R_a in µm	2.838	1.110	2.749	1.066
R_q in µm	3.445	1.391	3.394	1.328

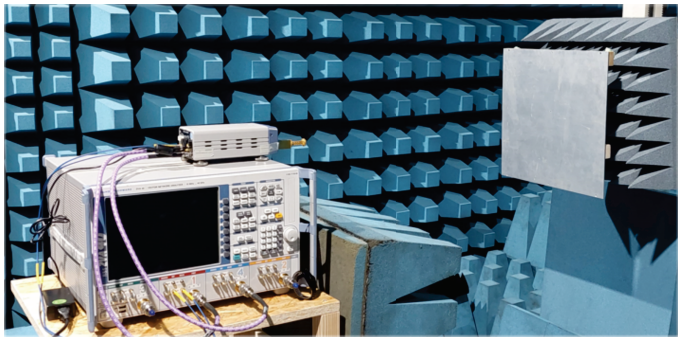

FIGURE 11. Utilized measurement setup in an anechoic chamber. The antenna is focused on the center of the mirror. The table with the analyzer can be rotated.

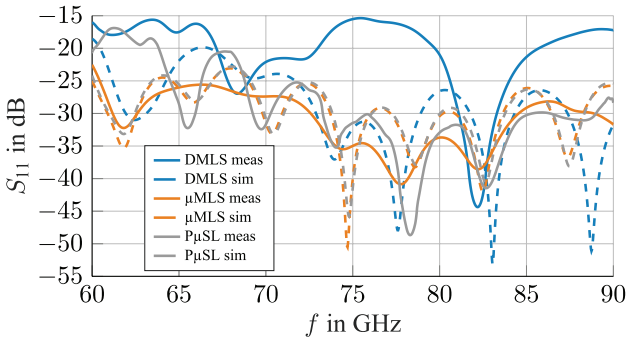

FIGURE 12. Reflection coefficients of manufactured corrugated horn antennas compared to simulation results.

TABLE 6. Comparison to other additive manufactured horn antennas.

Ref.	frequency	gain at center frequency	material	aperture efficiency	size (length × aperture diameter in mm)
[5] con.	60–90 GHz	24.5 dBi	Cu-15Sn polished	46.20 %	86.20 × 35.50 (measured)
[6] con.	50–75 GHz	20 dBi	316L	48.17 %	37.00 × 22.00 (design parameter)
[8] corr.	300 GHz	24.83 dBi	CuSn10+Au	30.77 %	28.36 × 10.00 (design parameter)
[10] con.	40–50 GHz	12 dBi	polymer+Cu	64.65 %	39.00 × 10.50 (design parameter)
[11] con.	24 GHz	17.319 dBi	18Ni300	43.86 %	46.98 × 44.10 (design parameter)
this work	60–90 GHz	13.1 dBi	316L	69.27 %	28.62 × 6.92 (measured)
this work	60–90 GHz	13 dBi	BMF HEK+Cu	60.94 %	28.28 × 7.28 (measured)
this work	60–90 GHz	12.5 dBi	$AlSi_{10}Mg$	57.43 %	28.81 × 7.08 (measured)

5. ANTENNA MEASUREMENT AND RESULTS

This section is about the antenna measurement and the discussion of the results. The measurement is conducted in an anechoic chamber using the Single-Antenna method.

5.1. Single-Antenna Method for Realized Gain Measurement

The Single-Antenna method, proposed in [24], is a variation of the Two-Antenna method from [21]. The advantage of the Single-Antenna method is that there is only one antenna and a rectangular reflector necessary for measuring the realized gain of this antenna. The reflection coefficient S_{11} of the antenna is measured with a vector network analyzer. After applying the inverse Fourier transform, timegating is used to remove unwanted reflections. Transforming back to the frequency domain, the ratio of received and transmitted power corresponds directly to the gated frequency response $|S_{11,\text{gated}}(f)|^2$. Inserting into Friis Free-Space-Transmission formula, the antenna gain can be calculated. At angles where the main beam is directed to the mirror edges, a significant error can occur due to scattering. A reference measurement with a standard gain horn from Eravant is conducted for verification. The measurement setup is depicted in Fig. 11. The absorbers are not perfectly suitable for this frequency range. Nevertheless, reference measurements show very good attenuation. The mirror has edge lengths of 42×45 mm, and the distance between the antenna and reflector was chosen to 80 cm. As very good measurement ranges achieve a gain measurement uncertainty of at least ± 0.2 dB for frequencies up to 40 GHz [25], a higher error in this measurement is expected.

5.2. Results

The obtained reflection coefficients of the corrugated horn antennas are provided in Fig. 12. The DMLS antenna shows higher reflections than the simulation results, which results from poor surface and corrugation quality. Both the PµSL and µMLS antennas are a good match to the simulation results, with the PµSL having a high deviation at lower fre-

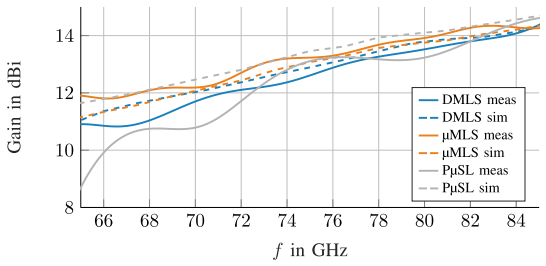

FIGURE 13. Gain versus frequency of manufactured corrugated horn antennas compared to simulation results. The frequency range is narrowed down due to high deviations at the borders resulting from timegating.

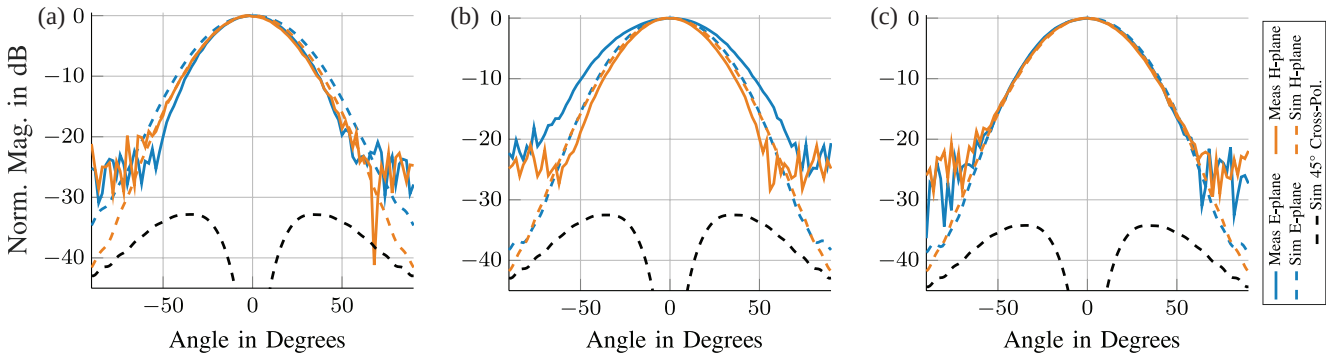

FIGURE 14. Gain patterns of (a) DMLS, (b) PµSL, and (c) µMLS corrugated horn antennas, normalized to maximum gain at 72 GHz.

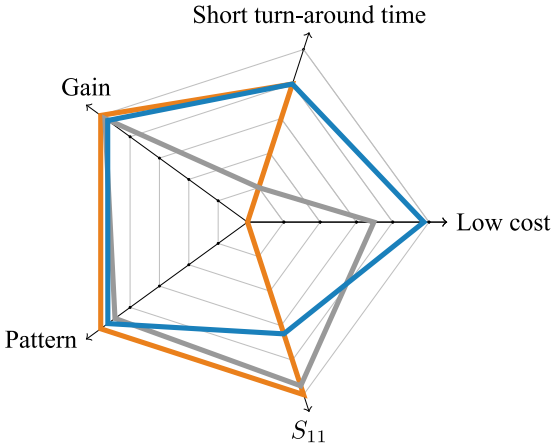

FIGURE 15. Result diagram. Measurement of S_{11}, gain, and pattern compared to simulation results via normalized cross-correlation. Turn-around time values: longer than 4 weeks, 3-4 weeks, 2-3 weeks, 1-2 weeks, less than 1 week (from the inside out). Cost values between 2500 and 0 euro (from the inside out).

quencies. Comparing the gain over frequency data depicted in Fig. 13, the metal printed antennas are similar to the simulation. Due to problems caused by timegating, which occur at the frequency borders, the gain frequency range is narrowed down to 65 to 85 GHz. The PµSL antenna shows deviations at low frequencies and approximates the simulation with increasing frequency. The achieved gain of the stainless steel antenna is higher than expected from the simulation. This observation can have multiple explanations, such as measurement inaccuracies or higher conductivity than assumed in simulation. E- and H-plane measurements, which can be seen in Fig. 14, are analyzed, and they are a good fit to the simulation results. The highest deviations arise at the E-plane pattern of the PµSL antenna, which can result from the high aperture tolerance measured before, whereas the best fitting is achieved by the µMLS antenna. The deviations at higher angles result from measurement inaccuracies. Additionally, the simulated cross-polarization pattern at a 45° cut-plane is included in the figures.

The performance is summarized in Fig. 15. The overall best performance was achieved by the 316L stainless steel horn, which was also the most expensive one. The high cost of 2500 € stands against an overall good match between simulation and measurement. The most significant advantage is the short turnaround time about a week. Furthermore, a metal plating of higher conductivity can be added to increase performance when using high conductivity and low relative permeability materials as discussed in [26], which also evens the slightly rough surface. On the contrary, an additional work step will be required.

The plastic antenna yields good results at a lower cost. Additional plating is necessary, which increases its turn-around time, in this case to four weeks. Furthermore, errors may occur when more complex structures are galvanized, as has happened with the SLA horn antenna. The low mechanical stability must also be considered, as thin parts tend to break even when a small force is applied. The PµSL antenna achieves good results regarding reflection coefficient and gain measurement. Again, the reflection curve fits the simulation very well. Due to tolerances and inaccuracies with the galvanization process, the pattern shows deviations between the simulation and measurement results, as seen in Fig. 14(b). With a price of 759 € the antenna yields a performance similar to the µMLS antenna for less cost, but with an additional processing step.

The aluminum DMLS horn is the cheapest one and shows the worst results. With the analysis of reflection coefficient in Fig. 12, the antenna shows −15 dB in the worst case. Even if this means higher reflections than that shown by the other antennas, it is sufficient for most applications. The gain curve and pattern show good results and match the simulation with small deviations, as seen in Figs. 13 and 14(a). This shows that the corrugations are of acceptable quality even with this coarse printing process. With a price of 70 € and a turnaround time about a week, these antennas are a good option for mass production.

6. CONCLUSION

The feasibility of using AM technologies to produce corrugated horn antennas is investigated. Of the standard printing technologies, SLA, PµSL, µMLS, and — with limitations — DMLS are identified as suitable for the 3D printing of corrugated horn antennas for the E-band. With plastic antennas, it must be ensured that electroplating is possible. The advantage of printed metal antennas is that post-processing of the surface is not necessary, but it can be used to further improve performance. Comparing the results to other proposed anten-

nas, similar performance is achieved without any further post-processing than necessary. Taking into account the results of the aluminum DMLS antenna, it can be seen that coarse-grained and high-tolerance printing processes can be suitable for printing antennas in the E-band with feature sizes about 200 µm. The slanted corrugations provide a self-stabilizing structure, which prevents sagging sufficiently. Therefore, slanted corrugations are a good choice for the vertical 3D printing of corrugated horn antennas. A short comparison to other additive manufactured antennas is given in Table 6. As can be seen, the antennas produced in this work provide similar performance to the others, in the case of the metal antennas without additional post-processing.

REFERENCES

[1] Diana, S., D. Brizi, C. Ciampalini, G. Nenna, and A. Monorchio, "A compact double-ridged horn antenna for ultra-wide band microwave imaging," *IEEE Open Journal of Antennas and Propagation*, Vol. 2, 738–745, 2021.

[2] Zoghi, M., F. Hodjatkashani, and M. E. Lajevardi, "A low distortion radiation pattern ultra-wideband TEM horn antenna," *IEEE Open Journal of Antennas and Propagation*, 1–1, 2024.

[3] Simionato, E., I. Aldaya, J. A. d. Oliveira, A. L. Jardini, J. Avila, G. S. d. Rosa, and R. A. Penchel, "Design guidelines and performance analysis of a wideband coaxial horn antenna fabricated via additive manufacturing," *IEEE Open Journal of Antennas and Propagation*, Vol. 5, No. 4, 1121–1132, 2024.

[4] Gu, C., Z. Zhang, F. Qin, F. Cheng, X. Shang, S. Cotton, J. Ullah, and A. Contreras, "A fully additive manufactured D-band SIW antenna," in *2024 18th European Conference on Antennas and Propagation (EuCAP)*, 1–5, Glasgow, United Kingdom, 2024.

[5] Zhang, B., Z. Zhan, Y. Cao, H. Gulan, P. Linnér, J. Sun, T. Zwick, and H. Zirath, "Metallic 3-D printed antennas for millimeter-and submillimeter wave applications," *IEEE Transactions on Terahertz Science and Technology*, Vol. 6, No. 4, 592–600, 2016.

[6] Zhang, B., P. Linnér, C. Karnfelt, P. L. Tarn, U. Södervall, and H. Zirath, "Attempt of the metallic 3D printing technology for millimeter-wave antenna implementations," in *2015 Asia-Pacific Microwave Conference (APMC)*, Vol. 2, 1–3, Nanjing, China, 2015.

[7] Kotzé, K. and J. Gilmore, "SLM 3D-printed horn antenna for satellite communications at X-band," in *2019 IEEE-APS Topical Conference on Antennas and Propagation in Wireless Communications (APWC)*, 148–153, Granada, Spain, 2019.

[8] Reinhardt, A., M. Möbius-Labinski, C. Asmus, A. Bauereiss, and M. Höft, "Additive manufacturing of 300 GHz corrugated horn antennas," in *2019 IEEE MTT-S International Microwave Workshop Series on Advanced Materials and Processes for RF and THz Applications (IMWS-AMP)*, 40–42, Bochum, Germany, 2019.

[9] Timbie, P. T., J. Grade, D. v. d. Weide, B. Maffei, and G. Pisano, "Stereolithographed MM-wave corrugated horn antennas," in *2011 International Conference on Infrared, Millimeter, and Terahertz Waves*, 1–3, Houston, TX, USA, 2011.

[10] Dorbath, B., K. Lomakin, T. Pfahler, J. Schür, and M. Vossiek, "Single-fed additively manufactured conical horn antenna with circular polarization for millimeter-wave applications," in *2023 17th European Conference on Antennas and Propagation (EuCAP)*, 1–5, Florence, Italy, 2023.

[11] Pereira, R. A. M., N. B. Carvalho, M. A. S. Costa, and J. M. M. Oliveira, "Additively manufactured 24 GHz circular horn antennas," in *2022 IEEE International Symposium on Antennas and Propagation and USNC-URSI Radio Science Meeting (AP-S/URSI)*, 1998–1999, Denver, CO, USA, 2022.

[12] Braasch, K., A. Teplyuk, D. Miek, J. Scheibler, T. Weißgärber, C. Zhong, and M. Höft, "Additive manufacturing of a copper elliptical corrugated horn antenna in the sub-terahertz regime," in *2024 IEEE/MTT-S International Microwave Symposium — IMS 2024*, 509–512, Washington, DC, USA, 2024.

[13] Gebhart, A., *Additive Fertigungsverfahren: Additive Manufacturing und 3D Drucken Drucken für Prototyping — Tooling — Produktion*, 2016.

[14] Din, E., "ISO/ASTM 52900: Additive Fertigung-Grundlagen-Terminologie," 2018.

[15] Zhang, B., Y.-X. Guo, H. Zirath, and Y. P. Zhang, "Investigation on 3-D-printing technologies for millimeter-wave and terahertz applications," *Proceedings of the IEEE*, Vol. 105, No. 4, 723–736, 2017.

[16] Protolabs, "Stereolithographie (SLA)," [Online]. Available: https://www.protolabs.com/de-de/services/3d-druck/ stereolithographie/. Accessed: 23.01.2023, 2023.

[17] "Dreigeist additive intelligence ogh," [Online] Available: https://www.dreigeist.com/mikro-3d-druck. Accessed: 23.01.2023, 2023.

[18] Protolabs, "Direktes Metall-Lasersintern," [Online]. Available: https://www.protolabs.com/de-de/services/3d-druck/direktes-metall-lasersintern/. Accessed: 23.01.2023, 2023.

[19] 3DMicroPrint GmbH, [Online]. Available: https://www.3dmicroprint.com/products/machines/dmp70series/. Accessed: 23.01.2023, 2023.

[20] 3DMicroPrint, "Material Data Sheet 316L Stainless Steel," 2022.

[21] Balanis, C. A., *Antenna Theory: Analysis and Design*, John Wiley & Sons, 2016.

[22] Granet, C. and G. L. James, "Design of corrugated horns: A primer," *IEEE Antennas & Propagation Magazine*, Vol. 47, No. 2, 76–84, 2005.

[23] Tafertshofer, M., M. Binder, and E. Biebl, "Evaluation of a metal 3D-printed corrugated conical horn antenna for the E-band," in *2023 IEEE International Conference on Microwaves, Communications, Antennas and Electronic Systems (COMCAS 2023)*, 2023.

[24] Krieger, J. D., E. H. Newman, and I. J. Gupta, "The single antenna method for the measurement of antenna gain and phase," *IEEE Transactions on Antennas and Propagation*, Vol. 54, No. 11, 3562–3565, 2006.

[25] Van Den Biggelaar, A. J., S. J. Geluk, B. F. Jamroz, D. F. Williams, A. B. Smolders, U. Johannsen, and L. A. Bronckers, "Accurate gain measurement technique for limited antenna separations," *IEEE Transactions on Antennas and Propagation*, Vol. 69, No. 10, 6772–6782, 2021.

[26] Genc, A., I. B. Basyigit, T. Goksu, and S. Helhel, "Investigation of the performances of X-Ku band 3D printing pyramidal horn antennas coated with the different metals," in *2017 10th International Conference on Electrical and Electronics Engineering (ELECO)*, 1012–1016, 2017.